

Proline Bulky Substituents Consecutively Act as Steric Hindrances and Directing Groups in a Michael/Conia-Ene Cascade Reaction under Synergistic Catalysis

Received 00th January 20xx,
Accepted 00th January 20xx

DOI: 10.1039/x0xx00000x

www.rsc.org/

Salil Putatunda,^{a†} Juan V. Alegre-Requena,^{b†} Marta Meazza,^c Michael Franc,^a Dominika Rohařová,^a Pooja Vemuri,^c Ivana Císařová,^d Raquel, P. Herrera,^{*b} Ramon Rios^{*c} and Jan Veselý^{*a}

In this study, we report a highly stereoselective and versatile synthesis of spiro pyrazolones, promising motifs that are being employed as pharmacophores. The new synthetic strategy merges organocatalysis and metal catalysis to create a synergistic catalysis using proline derivatives and Pd catalysts. This protocol is suitable for late-stage functionalization, which is very important in drug discovery. Additionally, a thorough computational study proved to be very useful to elucidate the function of the different catalysts along the reaction, showing a peculiar feature: the -CPh₂OSiMe₃ group of the proline catalyst switches its role during the reaction. In the initial Michael reaction, this group plays its commonly-assumed role of bulky blocking group, but the same group generates π -Pd interactions and acts as a directing group in the subsequent Pd-catalyzed Conia-Ene reaction. This finding might be very relevant especially for processes with many steps, such as cascade reactions, in which functional groups are assumed to play the same role during all reaction steps.

Introduction

The synthesis of highly complex scaffolds has long generated considerable research interest among organic chemists. Some of the most challenging organic structures to synthesize are spiro compounds (formally bicyclic organic compounds with rings connected through a quaternary atom centre).^{1–8} Spirocycles have unique structural properties due to their rigidity, and they are present in several natural products such as spongistatins, fredericamycin, the fused tetracyclic lycopodium alkaloid nankakurine **1** and alkaloid (-)-sibirine (**2**), and in pharmaceuticals (Figure 1).^{9,10} However, libraries of spiro compounds are still underrepresented in medicinal chemistry despite their usefulness as rigid conformations that reduce conformational entropy penalty when binding to pharmaceutical targets.^{9,10} Recent advances in synthetic methods have provided access to spiro building blocks, thereby slightly expanding their use in drug discovery. However, further synthetic work is clearly still needed because spirocycles are difficult to prepare. Their synthesis involves the formation of a

quaternary center, which is a challenging task in synthetic organic chemistry.

Recently, we have focused our efforts on developing enantioselective methods for the synthesis of spiro compounds through organocatalytic cascade reactions,^{11,12} using a synergistic approach.¹³ It is remarkable that synergistic catalysis has opened an exciting gate for the development of new reactions due to the possibility to activate two unreactive compounds at the same time.^{14,15}

Pyrazolones are a key class of five-membered ring nitrogen heterocycles, which have been used as pharmaceutical agents, agrochemicals, and chelating agents, among others.^{16,17} Pyrazole units are found in many natural products such as withasonine, pyrazofurin and formicin. Moreover, their use in pharmaceutical chemistry has increased due to their properties as p38 inhibitors and HIV integrase inhibitors.¹⁸ More specifically, spiro pyrazolones have been used as promising pharmacophores, showing potential as antitumor (**3**) and anti-inflammatory (**4**) agents (Figure 1).^{19–22} In our research group, we have investigated the synthesis of spiropyrazolones by organocatalytic procedures (Scheme 1)^{23,24} and very recently by a synergistic approach.²⁵

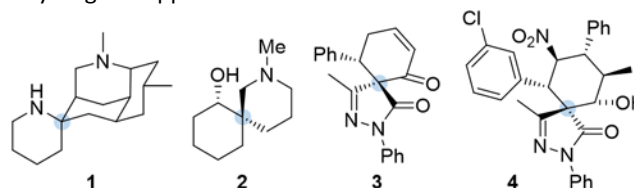


Figure 1. Spirocyclic natural products and pharmacophores.

To combine spiropyrazolone synthesis with synergistic catalysis, we focused on the venerable Conia-ene reaction as a viable

^a Department of Organic Chemistry, Faculty of Science, Charles University, Hlavova 2030, 128 43 Praha 2, Czech Republic. E-mail: jxvesely@natur.cuni.cz

^b Laboratorio de Organocatálisis Asimétrica, Departamento de Química Orgánica, Instituto de Síntesis Química y Catálisis Homogénea (ISQCH) CSIC-Universidad de Zaragoza, C/ Pedro Cerbuna 12, 50009 Zaragoza, Spain. E-mail: raquelph@unizar.es

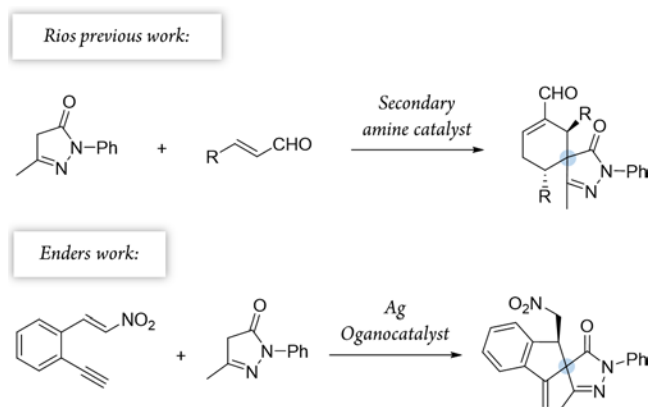
^c University of Southampton, School of Chemistry, Highfield Campus, SO17 1BJ, Southampton, UK. E-mail: rrt1f11@soton.ac.uk

^d Department of Inorganic Chemistry, Faculty of Science, Charles University, Hlavova 2030, 128 43 Praha 2, Czech Republic.

[†] These authors contributed equally to this work.

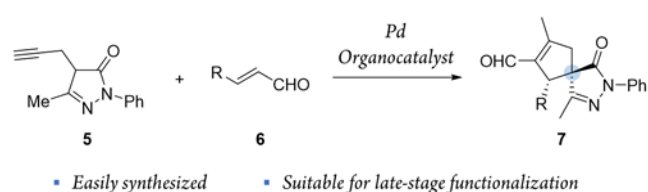
Electronic Supplementary Information (ESI) available, See DOI: 10.1039/x0xx00000x

synthetic tool to build five-membered (hetero) carbocycles.^{26,27} Previously, the Cordova's group developed a Conia-ene reaction to prepare spirooxindoles with excellent results^{28,29} and, more recently, Enders and colleagues reported the synthesis of spiropyrazolones by sequential organo- and silver catalysis.^{30,31} The latter involves a Michael/Conia-ene cascade reaction between pyrazolones and nitroalkenes bearing an alkyne (Scheme 1).



Scheme 1. Previously developed Michael/Conia-ene cascade reactions.

Inspired by these results, we envisioned a completely new strategy involving alkyne tethered pyrazolones **5** and enals **6** (Scheme 2). First, proline derived catalysts would be used to achieve a highly stereoselective activation of enals. Another reason to use this type of catalyst is that they preserve their catalytic activity even when metal Lewis acids, such as Pd, In and Ag, are also present in the reaction media.³²⁻³⁴ Moreover, we considered that this method could be easily applied to generate broad libraries of spiro compounds because enals **6** and pyrazolones **5** are easily synthesized and functionalized, and the compounds generated **7** contain several reactive groups (aldehydes, double bonds), thus enabling late-stage functionalization.



Scheme 2. New synergistic catalysis developed in this study to generate spiro pyrazolones **7**.

Moreover, the concurrent activation of both reactants through a synergistic catalysis allows a major reactivity scope and, at the same time, the use of simple catalysts that are not interconnected (in opposition to bifunctional catalysts³⁵⁻³⁷) (Figure 2). Additionally, these processes require less synthetic effort in the reaction optimization process because each catalyst can be individually optimized.

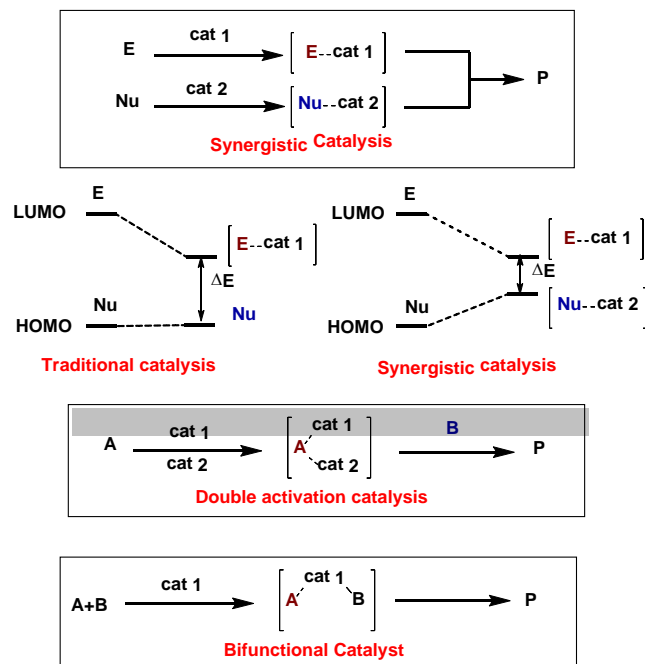


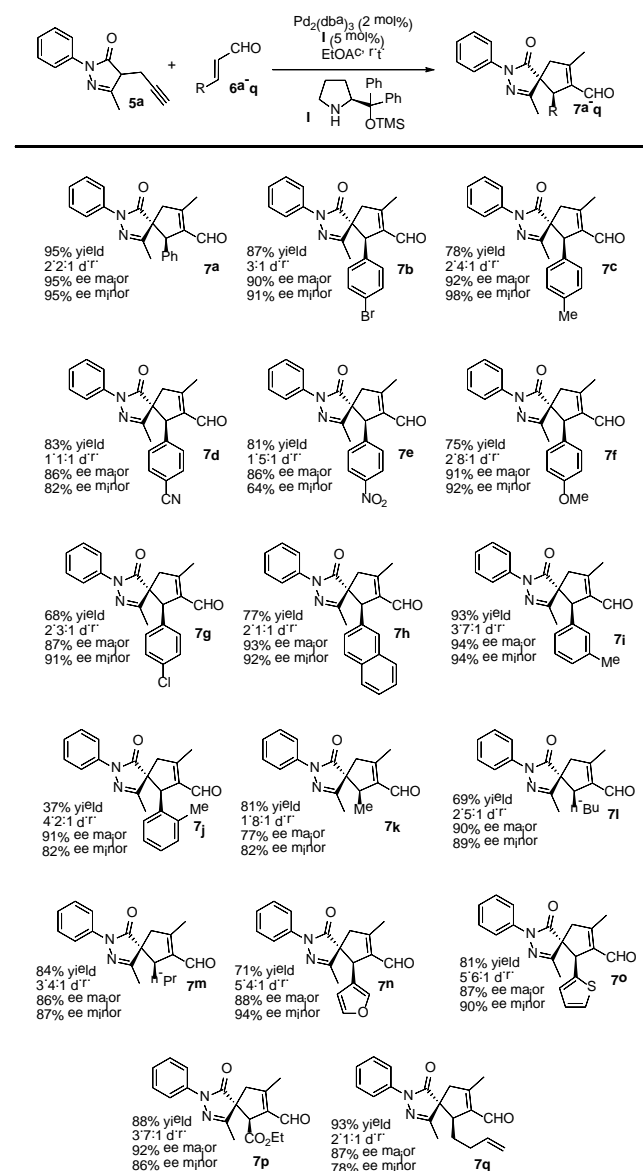
Figure 2. Synergistic catalysis against traditional and bifunctional catalysis.

Results and discussion

Synthetic results

After optimizing the model reaction, we achieved our best results when using ethyl acetate as the solvent, at room temperature, in the presence of 5 mol% TMS-protected diphenyl prolinol (**1**), acting as the secondary amine catalyst, and 2 mol% Pd₂(dba)₃ (see the ESI for more details about the optimization process). Remarkably, the reaction is catalyzed with a low organocatalyst loading (5 mol%), in contrast to similar organocatalytic reactions normally requiring 20 mol% of **1**. Moreover, without adding Pd, no cyclization reaction is detected, highlighting the importance of this synergistic cascade.

Thus, we studied the scope of this reaction using several enals **6** to demonstrate the general applicability of this synergistic cascade reaction (Scheme 3).

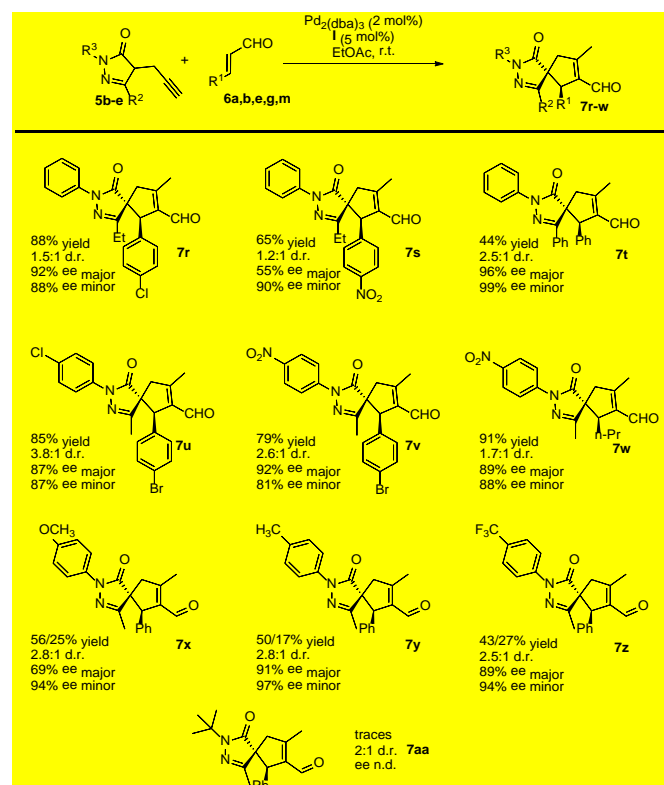


Scheme 3. Michael/Conia-ene cascade reaction between pyrazolone **5a** and enals **6a-q**.

In general, good-to-excellent yields of spiro compounds **7** with excellent enantioselectivities and moderate-to-good diastereoselectivities were assessed with different enals. The reaction is compatible with aliphatic enals (**7k**, **7l** and **7m**), with the glyoxylate derivative (**7p**), with dienals (**7q**), with aromatic enals with electron withdrawing groups (**7d**, **7e**) and with electron donating groups (**7c**, **7f**) in a *para* position on the aromatic ring. Moreover, *meta*-substituted aromatic enal (**7i**) and heteroaromatic enals (**7n** and **7o**) were prepared in excellent yields. As a general trend, heteroaromatics render final compounds **7** in higher diastereoselectivities (up to 5.6:1 d.r.) whereas spiro compound **7j** was formed in low yields when using the *ortho*-substituted cinnamic-type enal, most likely for steric reasons.

Subsequently, we studied the process using substituted pyrazolones **5b-e** (Scheme 4). The reaction is sensitive to steric effects of the pyrazolones. When the initial Me group on the pyrazolone moiety was changed to a Ph group, the reaction rate

significantly decreased. No full conversion was observed, even after a prolonged time (7 days), thus forming the corresponding product **7t** in low yields. In contrast, when Et substituted pyrazolones were used, the results were similar to previously reported values when using their Me-substituted analogues (**7r** vs **7g** and **7s** vs **7e**). We finally studied the effect of different R^3 substituents: the reaction works well with EWG, EDG and halogen as 4-substituent of the aromatic ring (**7u-z**), while low conversion was observed when R^3 is an aliphatic substituent (**7aa**).



Scheme 4. Catalyzed Michael/Conia-ene reaction between pyrazolones **5b-e** and enals **6a,b,e,g,m**.

The absolute configuration of final products was determined by X-ray diffraction analysis of compounds **8b** and **8b'** resulting from the oxidation of separated diastereoisomers of **7b** (Figure 3).³⁸ Based on the absolute configuration of major diastereomer **8b**, intermediate **Int-Ald** contains two stereocenters that will be referred to as (*S,R*) in the computational study.

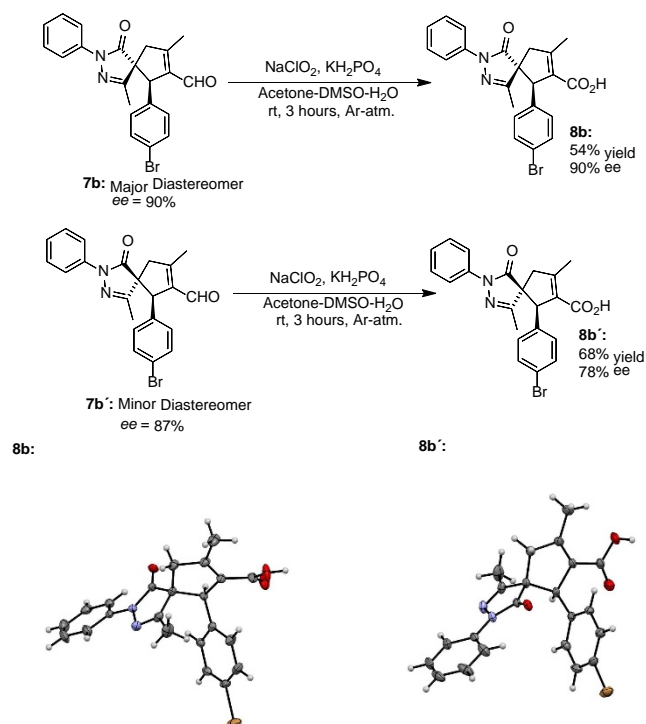
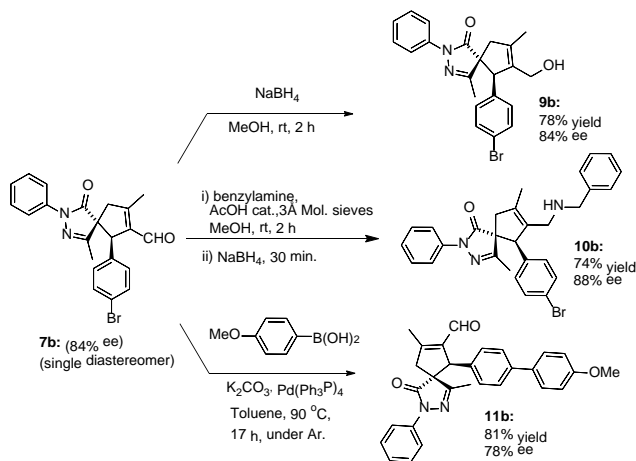


Figure 3. Synthesis and X-ray structure of **8b** and **8b'**.

The versatility of the reaction above has been demonstrated by late-stage derivatization of spiro compound **7b** (Scheme 5). Reduction and reductive amination of **7b**, used as a single diastereomer, afforded the corresponding alcohol **9b** and amine **10b**, respectively, in good yields, without losing enantiomeric purity. Similar results were found in Suzuki coupling with phenyl boronic acid, affording spiro compound **11b**, containing a biphenyl motif.



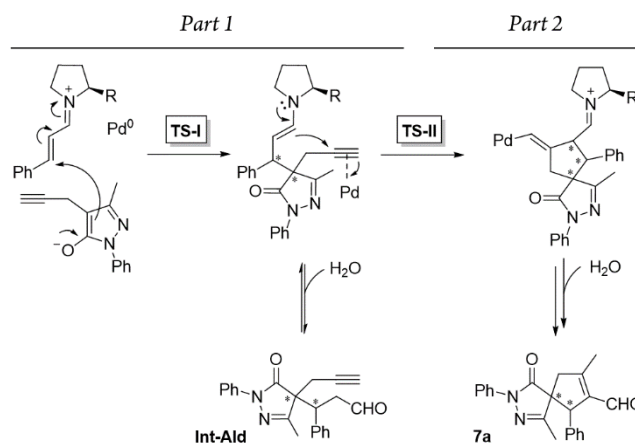
Scheme 5. Subsequent derivatizations of spiro compound **7b**.

Mechanistic studies

Initial experimental kinetic studies. **Initial experimental kinetic studies.** Before designing the computational study of this reaction,³⁹⁻⁴¹ different experiments were performed to collect data on mechanistic parameters of this process. Reaction kinetics assessed when using different amounts of the proline **1** and Pd catalysts were studied by NMR spectroscopy. These

experiments were carefully performed to achieve significant results because most of the Pd catalyst is not soluble in the reaction media (see the ESI for experimental details).

Additionally, we analyzed whether different parts of the reaction were reversible. The reaction was divided in two parts based on the two different C-C bond forming reactions (**TS-I** and **TS-II**) that occur during the whole process: **part 1**, including the Michael addition reaction that produces intermediate **Int-Ald**; and **part 2**, including the final Conia-ene reaction that generates product **7a** (Scheme 6).



Scheme 6. Summary of the reaction steps of this cascade reaction divided into two parts based on the different C-C bond-forming reactions.

To study the reversibility of the different parts of the reaction, several variable temperature NMR experiments were conducted. In the first experiment, the reaction was performed without adding the Pd catalyst, and the Michael reaction (**part 1**) stopped before the initial reagents were completely consumed. When the reaction stopped (at 62% of cinnamaldehyde conversion, entry 1), we changed the temperature of the reaction mixture and analyzed how temperature variations affected the conversion (percentage) and diastereomeric ratio (dr) of intermediate **Int-Ald** (Table 1, entries 1-5 and Figure S3).

Table 1. Conversion of cinnamaldehyde (**6a**) in the Michael (entries 1-6) and cascade reaction (entries 7-11) and dr of intermediate **Int-Ald** or product **7a** at different temperatures.

Entry ^a	Substrate	T (K)	dr	Conversion (%)
1	Int-Ald	298	1:3.4	62
2	Int-Ald	308	1:3.3	55
3	Int-Ald	318	1:3.1	46
4	Int-Ald	328	1:2.9	40
5 ^b	Int-Ald	298	1:3.4	62
6 ^c	Int-Ald	298	1:3.4	-
7	7a	298	1:6.1	100
8	7a	308	1:6.0	100
9	7a	318	1:6.1	100
10	7a	328	1:6.0	100
11 ^c	7a	298	1:1.5	-

^a See the ESI for the reaction conditions of the kinetic experiments.

^b After cooling down the reaction from 328 K to 298 K.

^c Using pyrrolidine as the catalyst.

The results indicated that changes in temperature affected both conversion and dr. Interestingly, the variations in these parameters were reversible because, when the reaction was cooled down from 328 K to rt, the initial conversion and dr were observed again within 5-10 minutes (Table 1, entry 5). Furthermore, when pyrrolidine was used as the catalyst, the same dr was observed at rt although this catalyst is not chiral (Table 1, entries 1 and 6). These results suggest that this Michael reaction is reversible and that the conversion and dr are primarily determined by the energy of the different diastereomers of **Int-Ald** (thermodynamically controlled stereoselectivity)⁴¹ rather than the energy of the transition states of C-C bond formation (**TS-I**, kinetically controlled stereoselectivity).

Similarly, we performed variable temperature NMR experiments using reactions containing both catalysts (**I** and Pd) and, therefore, leading to product **7a** (Table 1, entries 7-10). In contrast to the previous experiments, we observed no retro-Conia-ene reaction or variations in the dr of product **7a** at any temperature tested (Table 1 and Figure S4). Moreover, when pyrrolidine was used as the catalyst at rt, the dr of the product showed a significant change in comparison with the corresponding chiral reaction (Table 1, entries 7 and 11). These two findings suggest that the second part of the overall process is irreversible at the range of temperatures tested, thus indicating a Curtin–Hammett scenario (kinetically controlled stereoselectivity).⁴²

To identify the rate- and enantio-determining steps, we analyzed the concentration profiles of the different reaction components. As previously observed, when the equilibrium of **part 1** is reached, cinnamaldehyde (**6a**) conversion is 62%, and intermediate **Int-Ald** has an equilibrium concentration of 0.098 M (marked with an "X" next to the Y axis). Figure 4 shows that

intermediate **Int-Ald** reacts quickly and generates product **7a** before reaching the equilibrium concentration. This suggests that the slowest part of the reaction is **part 1**.

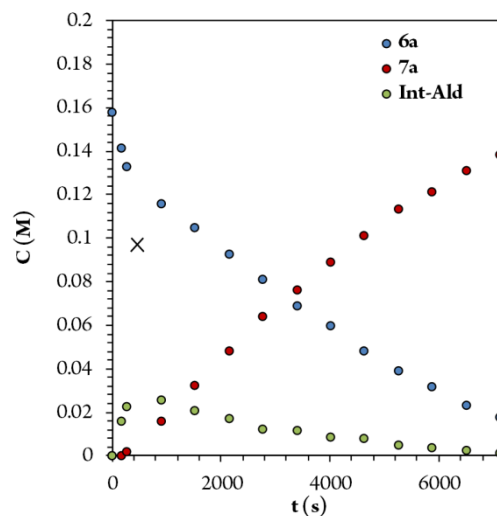
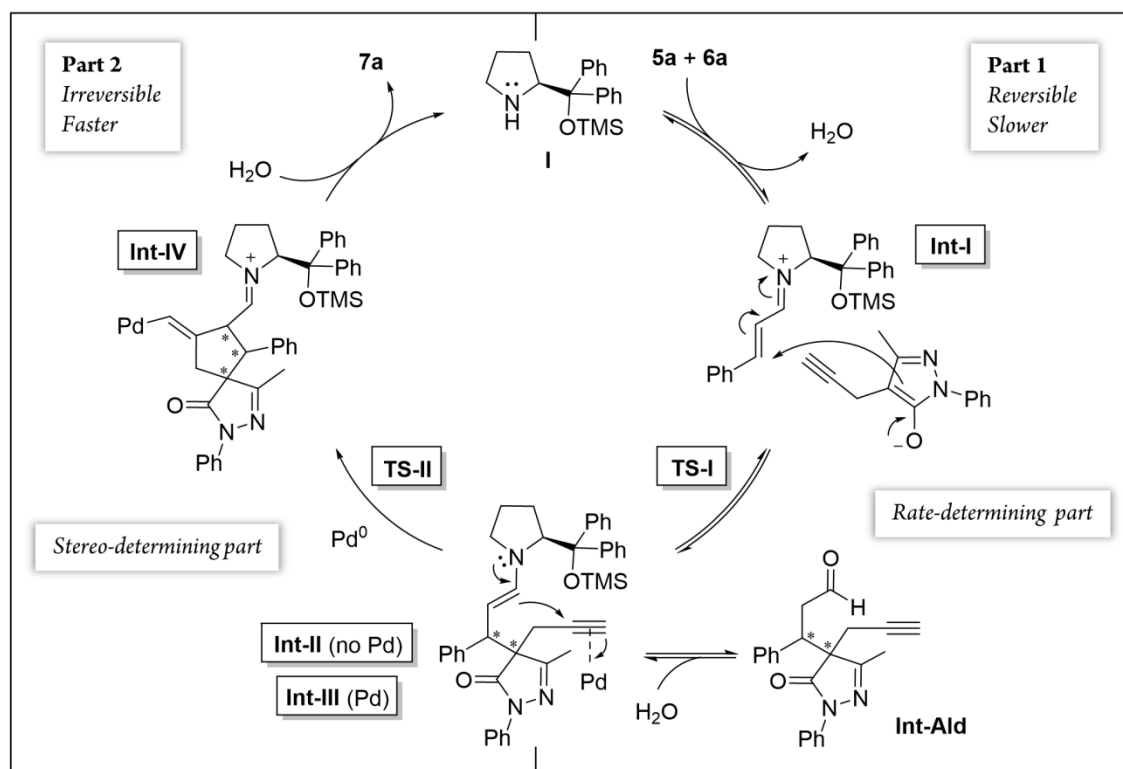


Figure 4. Concentration of the different reaction components over time.

Although the stereocenters of the reactions are formed in **part 1**, diastereoselectivity changes from the intermediate **Int-Ald**, formed in **part 1**, to the final product **7a**, formed in **part 2**. The results from the kinetic studies suggest that (1) **part 1** is slower than **part 2** and that (2) the diastereoselectivity of the final product is determined in **part 2**. Thus, although **part 1** contains the rate-limiting step (or steps), **part 2** contains the stereo-determining step because the reactions of **part 1** are reversible whereas at least one reaction of **part 2** is irreversible. Accordingly, we designed a catalytic cycle based on all the data gathered in the kinetic studies (Scheme 7).



Scheme 7. General catalytic cycle of the cascade reaction studied.

Computational study.⁴³

After the initial kinetic experiments, the reaction mechanism was computationally studied. All the calculations were performed at the ω B97X-D/Def2-QZVPP(SMD)(UFgrid)// ω B97X-D/6-311G(d)(SMD)(UF grid) level (using the Def2-TZVP basis set for Pd atoms instead of the 6-311G(d) basis set in geometry optimizations). ω B97X-D is a highly reliable functional in similar reactions with many noncovalent interactions.⁴⁴⁻⁴⁶ Moreover, we tested the validity of this computational approach in generating reliable structures by optimizing, using ω B97X-D/6-311G(d)(SMD)(UF grid), the geometry of a X-ray structure of the condensation product of proline **I** and cinnamaldehyde (**6a**).⁴⁷ In this analysis, we found

no significant structural differences between the computationally optimized structure and its corresponding crystal structure (see the ESI for more information). First, the energies of the first C-C bond forming step (**TS-I**) were calculated (Figure 5). As explained above, even though the stereocenters are formed in this step (**TS-I**), this transition state does not determine the final stereoselectivity (*S,R*) of product **7a**. From the previous experiments, three important aspects of **part 1** can be remarked: this part proceeds even when Pd is not added to the reaction; there is much more proline **I** in the reaction media than Pd; and the reaction rate does not vary in a great extent when Pd is added. Therefore, we can assume that most of the reaction pathways of **part 1** and, therefore, most of the **TS-I** steps probably proceed without the Pd atom.

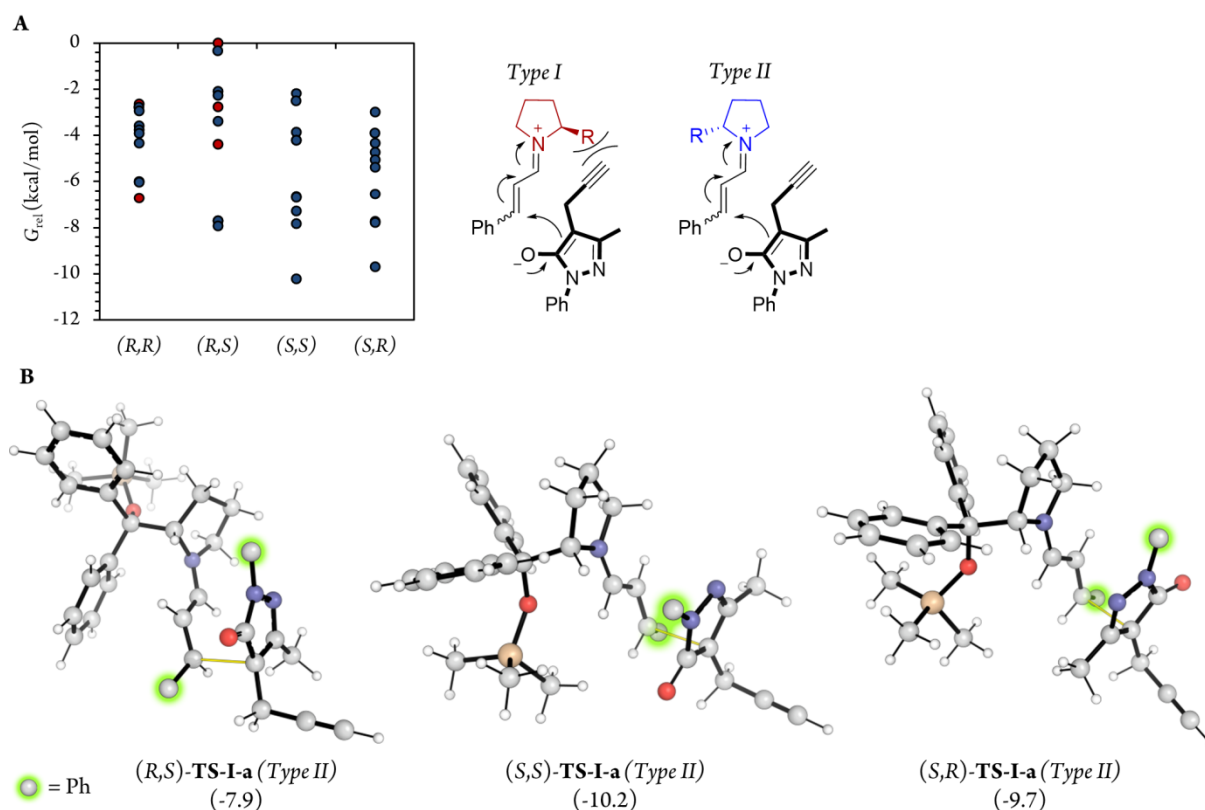


Figure 5. (A) Relative G of the 10 most stable conformations of the **TS-I** step of each diastereoisomer, using the same point (least stable conformer, (R,S)-**TS-I-j**) as the reference in all cases and in different types of attack. Dots represent the energies of the different individual conformations. (B) Images of the most relevant **TS-I** steps, showing the C-C bond formation coordinates with thin yellow lines. 54 different conformations were analyzed for each diastereomer (216 conformations in total).

Although no information on the stereoselectivity of final product **7a** can be extracted from this study, a few common trends were observed among the most favorable **TS-I** steps of all diastereomers. Most importantly, the most stable **TS-I** steps lead to Michael reactions that occur on the opposite side of the proline substituent (-CPh₂OTMS), as previously proposed by other authors (Figure 5A, Type II attack).⁴⁸ Furthermore, no significant noncovalent interactions occur between this group of the catalyst and the attacking pyrazolone group (**5a**). Therefore, the -CPh₂OTMS group of the proline sterically

hinders the approach of **5a** to the side of the proline in which this blocking group is located.⁴⁷

In addition, for further insight into the two C-C bond forming reactions (Figure 6), we calculated Boltzmann averaged energies of the **Int-I**, **Int-II**, **Int-III**, **TS-II** and **Int-IV** systems of the (S,R) diastereomer, the major diastereomer of product **7a** observed experimentally. Using Boltzmann averaged energies of the different reaction coordinates is a useful strategy that has been previously applied to study the global mechanism of systems with multiple possible conformations.⁴⁹

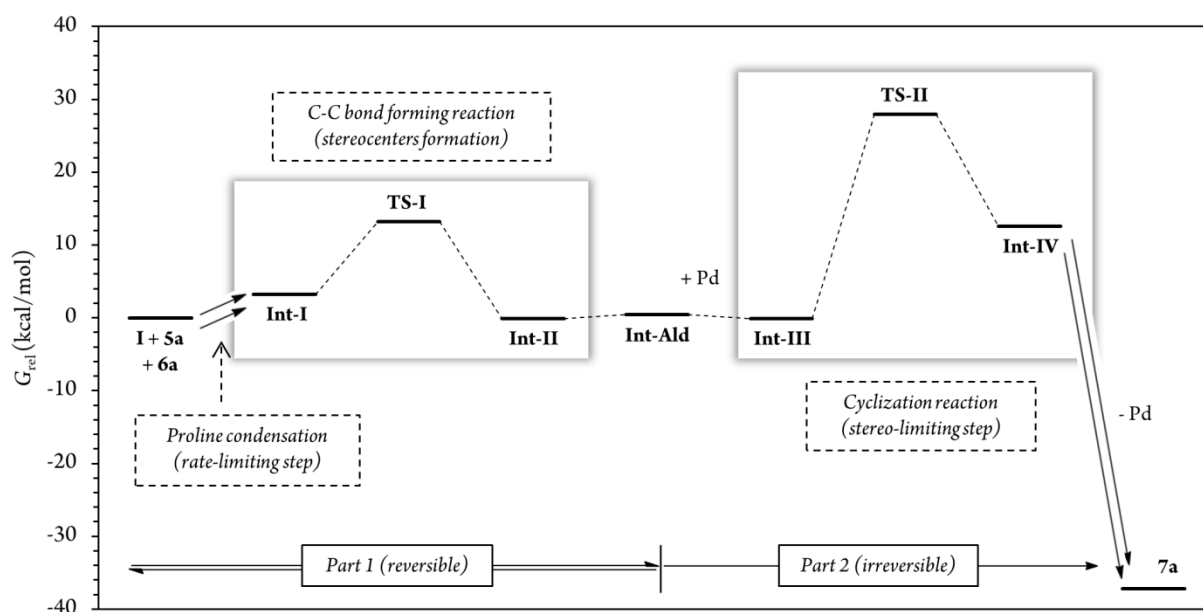


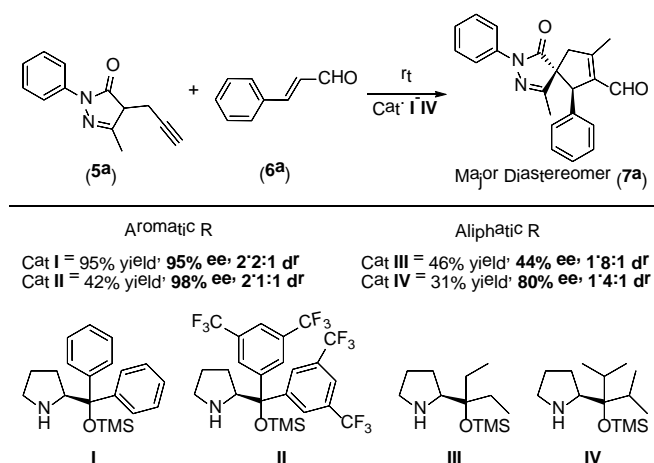
Figure 6. Relative Gibbs free energies along the (*S,R*) reaction coordinate (for more information see section *G of the Calculations* of the ESI). For this energy profile, we used Boltzmann average *G* of the 10 most stable conformations of each reaction step. A total of 54 different conformations were analyzed for steps **Int-I**, **TS-I** and **Int-II**, and 62 conformations for steps **Int-III**, **TS-II** and **Int-IV**.

The calculations predicted that the *G* necessary to promote the retro-Michael reaction of **part 1** (from aldehyde **Int-Ald** to **TS-I**) is much lower than that required for the retro-Conia-ene reaction of **part 2** (from final product **7a** to **TS-II**). In fact, the retro-Conia-ene reaction shows an activation *G* of 65.2 kcal/mol, which suggests that this retro-cyclization process is extremely slow at rt. This is in line with the initial experimental findings suggesting that **part 1** is reversible, whereas **part 2** is irreversible.

The experimental results showed that the rate-limiting step was enclosed in **part 1** of the mechanism; however, the reaction coordinates from the computational study indicated that step **TS-II** (cyclization step), from **part 2**, had a much higher energy than **TS-I** (Michael addition). This difference suggests that the rate-limiting step is included in the initial iminium formation prior to the Michael reaction which agrees with the study conducted by Moliner, Luk and colleagues. These authors showed a relatively high *G* activation barrier of approximately 28 kcal/mol in the iminium formation between a proline derivative and cinnamaldehyde of a Henry reaction in various solvents.⁴⁹ Additionally, when we followed the reaction by ¹H-NMR experiments, we could not detect condensation products from catalyst **I** and cinnamaldehyde **6a**, that is, no iminium ion intermediate is neither accumulated nor detected before the Michael addition (Figures S5-6). This strongly suggests that the subsequent step, the Michael addition reaction, is faster than the initial proline condensation with cinnamaldehyde **6a**. Thus, the *in situ* generated iminium ion intermediate would be rapidly consume in the next step and consequently, not detected by NMR. Therefore, the NMR results from this study (Figures 4 and S5-6) are in line with the computational energy profile calculated and indicate that the initial prolinol condensation with cinnamaldehyde **6a** is the rate-limiting step of the process.

Notably, in the most favorable **TS-II** step, the CPh₂OTMS group of proline **I** acts as a directing group due to a favorable π -Pd interaction (Figure 7, *Type III* and *IV*), whereas this substituent acted as a blocking group in **TS-I**. This is an interesting example of a reaction in which one of the groups of the catalyst acts as a sterically hindered substituent in one part of the mechanism and as a directing group in the subsequent part. Hence, this finding highlights the importance of computational mechanistic studies, especially in multi-step reactions since researchers often assume that a specific functional group always plays the same role during the whole reaction.

Therefore, based on the computational results of **TS-II**, the stereoselective-limiting step, if the catalyst does not contain any aromatic group to coordinate with Pd the stereoselectivity obtained should change in a great extent. As expected, modifications of the aromatic ring of the catalyst led to similar enantioselectivities and diastereoselectivity (Scheme 8, **I** and **II**). In contrast, when the aromatic rings are replaced for aliphatic chains the stereoselectivity dropped considerably (Scheme 8, **III** and **IV**). These experimental results are in line with the computational outcomes and support that the aromatic rings are coordinated to Pd during the cyclization step. On the other hand, the reactivity observed with each catalyst is intrinsic to each structure and directly related only with their structure-reactivity profile shown in **part 1** of the mechanism (the rate-limiting step).



Scheme 8. Experimental results using catalysts I-IV.

Finally, to further validate the method by comparing more experimental and theoretical results, we calculated the G of both *syn*- and *anti*-**Int-Ald**, the compound that controls the selectivity of **part 1**. Experimentally, we observed 38% cinamaldehyde and 62% **Int-Ald** in the equilibrium at rt, which corresponds to a difference in G (ΔG) of -1.7 kcal/mol between the G of the initial products and the G of **Int-Ald**. Computationally, the ΔG between diastereomer **Int-Ald** and the initial reagents is -0.4 kcal/mol, which shows a very low margin of error (1.3 kcal/mol) in comparison with the experimental result (see *Calculation of the dr in the Equilibrium of Part 1* section in ESI for more information).

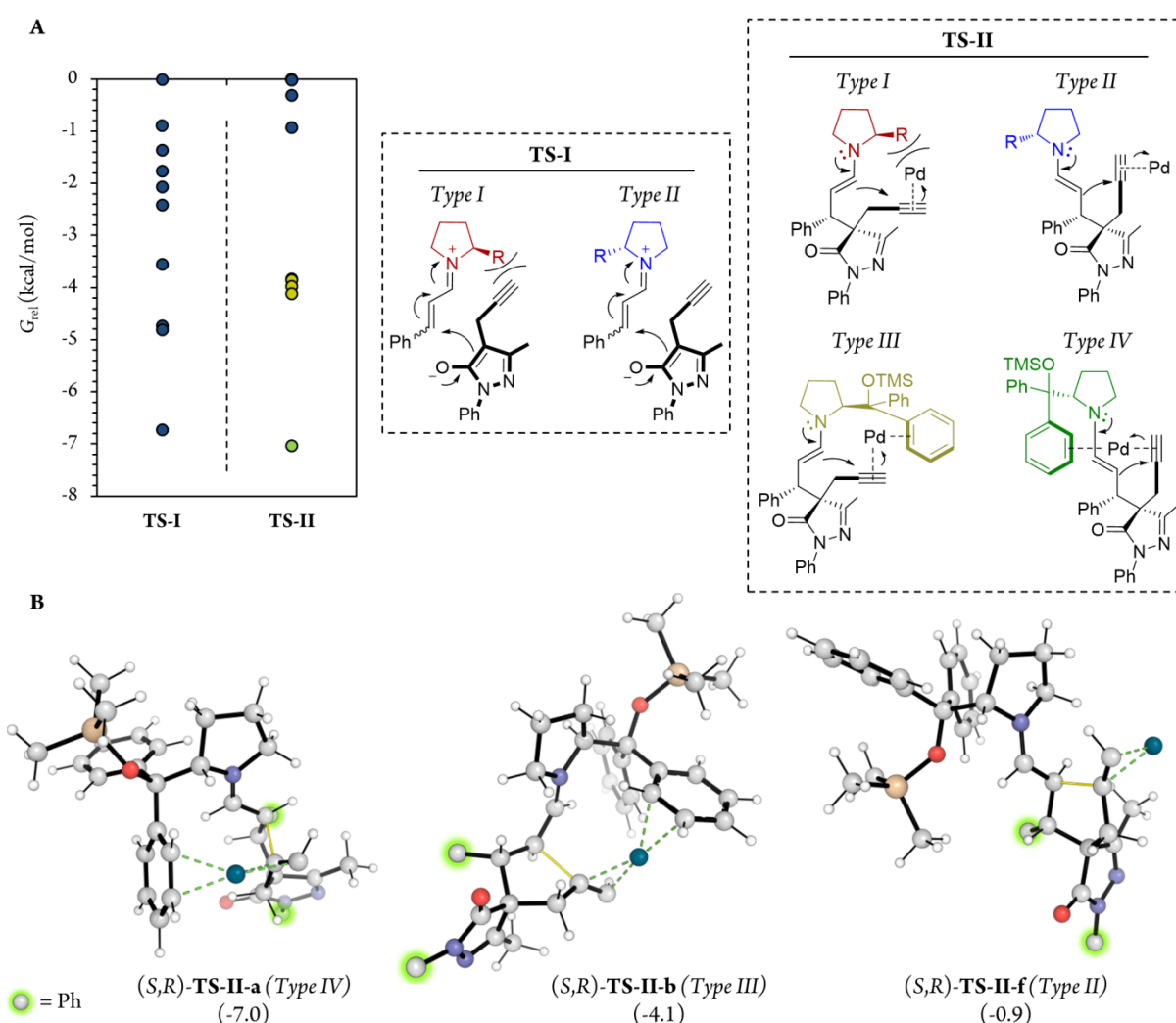


Figure 7. (A) Energies of the (S,R)-TS-I and (S,R)-TS-II step along with the different types of attack in each transition state. Dots represent the relative energies of the 10 most stable conformations using the least stable conformers (TS-I-j and TS-II-j, respectively) as the reference for TS-I and TS-II. (B) Representation of the most favourable TS-II step of attack types I to IV (TS-II-a, TS-II-b and TS-II-f), showing C-C bond formation coordinates with thin yellow lines and π -Pd interactions with dashed green lines.

Conflicts of interest

There are no conflicts to declare.

Acknowledgements

R. P. H. and J. V. A.-R. thank Ministerio de Economía, Industria y Competitividad (CTQ2017-88091-P) and Gobierno de Aragón-

Fondo Social Europeo (E07_17R) for funding their re-search. All calculations were performed at the Trueno cluster facility, SGAI-CSIC. J. V. A.-R. thanks Dr. R. Paton for his help with the script to generate the PyMol style and GoodVibes. S. P. and J. V. thank the Czech Science Foundation (No 18-20645S) for funding the study, Dr. Hybelbauerová and Dr. Tošner for providing the NMR service, Dr. Štícha for providing the MS analysis and Dr. Carlos V. Melo for proofreading the manuscript. **M. M. and R. R. are grateful for EPSRC Core Capability Funding (EP/K039466/1). RR thanks Alessandra Carnero for initial studies.**

Notes and references

- R. Rios, *Chem Soc. Rev.*, 2012, **41**, 1060.
- D. Cheng, Y. Ishihara, B. Tan and C. F. Barbas III, *ACS Catal.*, 2014, **4**, 743.
- Z.-Y. Cao and J. Zhou, *Org. Chem. Front.*, 2015, **2**, 849.
- L.-J. Yan and Y.-C. Wang, *ChemistrySelect*, 2016, **1**, 6948.
- S. Kotha, N. R. Panguluri and R. Ali, *Eur. J. Org. Chem.*, 2017, 5316.
- X. Xie, W. Huang, C. Peng and B. Han, *Adv. Synth. Catal.*, 2018, **360**, 194.
- J. Guang-Mei and F. Shi, *Chem. Commun.*, 2018, **54**, 6607.
- X. Fang and C.-J. Wang, *Org. Biomol. Chem.*, 2018, **16**, 2591.
- Y. Zheng, C. M. Tice and S. B. Singh, *Bioorg. Med. Chem. Lett.*, 2014, **24**, 3673.
- T. L. Pavlovskaya, R. Gr. Redkin, V. V. Lipson and D. V. Atamanuk, *Mol. Divers.*, 2016, **20**, 299.
- P.-Y. Géant, M. Urban, M. Remeš, I. Císařová and J. Veselý, *Eur. J. Org. Chem.*, 2013, 7979.
- X. Companyó, A. Zea, A.-N. R. Alba, A. Mazzanti, A. Moyano and R. Rios, *Chem. Commun.*, 2010, **46**, 6953.
- M. Meazza and R. Rios, *Chem. Eur. J.*, 2016, **22**, 9923.
- A. E. Allen and D. W. C. MacMillan, *Chem. Sci.*, 2012, **3**, 633.
- a) M. Meazza and R. Rios, *Synthesis*, 2016, 960; b) S. Afewerki and A. Cordova, *Chem. Rev.* 2016, **116**, 13512.
- Pyrazol-3-ones. Part IV: Synthesis and Applications. G. Varvounis, *Adv. Heterocyclic Chem.* (Ed: Katritzky, A. R.), Academic Press 2009, **98**, 143.
- P. Chauhan, S. Mahajan and D. Enders, *Chem. Commun.*, 2015, **51**, 12890.
- V. Hadi, Y. Koh, T. W. Sanchez, D. Barrios, N. Neamati and K. W. Jung, *Bio. Med. Chem. Lett.*, 2010, **20**, 6854.
- Y. L. Janin, *Bioorg. Med. Chem.*, 2007, **15**, 2479.
- M.-T. Gutierrez-Lugo and C. Bewley, *J. Med. Chem.*, 2008, **51**, 2606.
- I. R. Matthews, *PCT Int. Appl. WO 46679*, 2005.
- A. Kimata, H. Nakagawa, R. Ohyama, T. Fukuuchi, S. Ohta, T. Suzuki and N. Miyata, *J. Med. Chem.*, 2007, **50**, 5053.
- A. Zea, A.-N. R. Alba, A. Mazzanti, A. Moyano and R. Rios, *Org. Biomol. Chem.*, 2011, **9**, 6519.
- A. Zea, A.-N. R. Alba, G. Valero, T. Calbet, M. Font-Bardia, A. Moyano and R. Rios, *Eur. J. Org. Chem.*, 2011, 2053.
- M. Meazza, M. Kamlar, L. Jašíková, B. Formánek, A. Mazzanti, J. Roithová, J. Veselý and R. Rios, *Chem. Sci.*, 2018, **9**, 6368.
- For an excellent recent review regarding Conia-ene reactions, see: D. Hack, M. Blumel, P. Chauhan, A. R. Phillips and D. Enders, *Chem. Soc. Rev.*, 2015, **44**, 6059.
- For an example of cooperative catalysis to develop this reaction, see: T. Yang, A. Ferrali, F. Sladojevich, L. Campbell and D. J. Dixon, *J. Am. Chem. Soc.*, 2009, **131**, 9140.
- a) C. Xu, L. Deiana, S. Afewerki, C. Incerti-Pradillos, O. Cordova, P. Guo, A. Cordova and N. Hedin, *Adv. Synth. Catal.* 2015, **357**, 2150; b) L. Deiana, Y. Jiang, C. Palo-Nieto, S. Afewerki, C. A. Incerti-Pradillos, O. Verho, C.-W. Tai, E. V. Johnston and A. Cordova, *Angew. Chem. Int. Ed.*, 2014, **53**, 3447;
- L. Deiana, L. Ghisu, S. Afewerki, O. Verho, E. V. Johnston, N. Hedin, Z. Bacsik and A. Cordova, *Adv. Synth. Catal.*, 2014, **56**, 2485.
- D. Hack, P. Chauhan, K. Deckers, M. Yusuke, G. Raabe and D. Enders, *Chem. Commun.*, 2015, **51**, 2266.
- D. Hack, K. Deckers, P. Chauhan, N. Selling, L. Rue-benach, L. Mertens, F. Schoenebeck and D. Enders, *Angew. Chem. Int. Ed.*, 2016, **55**, 1797.
- M. Meazza, M. E. Light, A. Mazzanti and R. Rios, *Chem. Sci.*, 2016, **7**, 984.
- M. Meazza, V. Ceban, M. B. Pitak, S. J. Coles and R. Rios, *Chem. Eur. J.*, 2014, **20**, 16853.
- V. Ceban, P. Putaj, M. Meazza, M. B. Pitak, S. J. Coles, J. Veselý and R. Rios, *Chem. Commun.*, 2014, **50**, 7447.
- H. Miyabe and Y. Takemoto, *Bull. Chem. Soc. Jpn.*, 2008, **81**, 785.
- S. J. Connon, *Chem. Commun.*, 2008, 2499.
- I. G. Sonsona, E. Marqués-López and R. P. Herrera, *Beilstein J. Org. Chem.*, 2016, **12**, 505.
- Crystallographic data have been deposited with Cambridge Crystallographic Data Centre: Deposit number: CCDC 1859005 and 1859006 for **8b** and **8b'**, respectively.
- F. Sladojevich, A. L. Fuentes de Arriba, I. Ortín, T. Yang, A. Ferrali, R. S. Paton and D. J. Dixon, *Chem. Eur. J.*, 2013, **19**, 14286.
- S. Santoro, L. Deiana, G.-L. Zhao, S. Lin, F. Himo and A. Córdoba, *ACS Catal.*, 2014, **4**, 4474 and references therein.
- For other mechanistic studies using proline **I**, see also: K. S. Halskov, B. S. Donslund, B. M. Paz and K. A. Jørgensen, *Acc. Chem. Res.*, 2016, **49**, 974.
- Q. Peng, F. Duarte and R. S. Paton, *Chem. Soc. Rev.*, 2016, **45**, 6093.
- M. J. Frisch, G. W. Trucks, H. B. Schlegel, G. E. Scuseria, M. A. Robb, J. R. Cheeseman, G. Scalmani, V. Barone, B. Mennucci, G. A. Petersson, H. Nakatsuji, M. Caricato, X. Li, H. P. Hratchian, A. F. Izmaylov, J. Bloino, G. Zheng, J. L. Sonnenberg, M. Hada, M. Ehara, K. Toyota, R. Fukuda, J. Hasegawa, M. Ishida, T. Nakajima, Y. Honda, O. Kitao, H. Nakai, T. Vreven, J. A. Jr Montgomery, J. E. Peralta, F. Ogliaro, M. Bearpark, J. J. Heyd, E. Brothers, K. N. Kudin, V. N. Staroverov, R. Kobayashi, J. Normand, K. Raghavachari, A. Rendell, J. C. Burant, S. S. Iyengar, J. Tomasi, M. Cossi, N. Rega, J. M. Millam, M. Klene, J. E. Knox, J. B. Cross, V. Bakken, C. Adamo, J. Jaramillo, R. Gomperts, R. E. Stratmann, O. Yazyev, A. J. Austin, R. Cammi, C. Pomelli, J. W. Ochterski, R. L. Martin, K. Morokuma, V. G. Zakrzewski, G. A. Voth, P. Salvador, J. J. Dannenberg, S. Dapprich, A. D. Daniels, O. Farkas, J. B. Foresman, J. V. Ortiz, J. Cioslowski and D. J. Fox, Gaussian 09, Revision D.01; Gaussian, Inc., Wallingford CT, 2016.
- A. D. Becke, *J. Chem. Phys.*, 1997, **107**, 8554.
- J.-D. Chai and M. Head-Gordon, *Phys. Chem. Chem. Phys.*, 2008, **10**, 6615.
- L. Goerigk and S. A. Grimme, *Phys. Chem. Chem. Phys.*, 2011, **13**, 6670.
- U. Grošelj, D. Seebach, D. M. Badine, W. B. Schweizer, A. K. Beck, I. Krossing, P. Klose, Y. Hayashi and T. Uchimaru, *Helv. Chim. Acta*, 2009, **92**, 1225.
- E. Marqués-López and R. P. Herrera, *Curr. Org. Chem.*, 2011, **15**, 2311 and references therein.
- E. Lyngvi, J. W. Bode and F. A. Schoenebeck, *Chem. Sci.*, 2012, **3**, 2346.
- K. Świderek, A. R. Nödling, Y.-H. Tsai, L. Y. P. Luk and V. Moliner, *J. Phys. Chem. A*, 2018, **44**, 451.